Early postnatal moderate catch-up growth in rats with nutritional intrauterine growth restriction preserves pulmonary vascular and cognitive function in adulthood

LIXIA YE, YAJIE HUANG, KEWEI CHEN, CHENGCHENG HANG, YUHAN YING, LU ZU, XIAOFEI LUO and LIZHONG DU

Department of Neonatology, Children's Hospital, Zhejiang University School of Medicine, Hangzhou, Zhejiang 310052, P.R. China

Received October 25, 2023; Accepted February 9, 2024

DOI: 10.3892/etm.2024.12471

Abstract. Intrauterine growth restriction (IUGR) with rapid postnatal catch-up growth is strongly associated with pulmonary vascular dysfunction in adulthood, whereas IUGR with delayed growth in early postnatal life results in long-term brain deficits. In the present study, it was hypothesized that IUGR with early moderate catch-up growth may alleviate pulmonary vascular remodeling in adulthood without affecting memory function. An IUGR model was established by restricting maternal nutrition during pregnancy. Different growth patterns were achieved by adjusting the litter size in each group during lactation. Rats meeting the weight requirement at weaning were selected for subsequent studies at three time points (3, 9 and 13 weeks). Cognitive function was evaluated using a Y-maze. Invasive hemodynamic measurements were conducted to measure the mean pulmonary arterial pressure (mPAP). In addition, primary pulmonary artery smooth muscle cells (PASMCs) and pulmonary vascular endothelial cells (PVECs) were cultured to investigate their role in the increase in mPAP following rapid catch-up growth. The results showed that memory function deficits in the rats in the delayed growth group were associated with reduced proliferation of neural stem cells in the subgranular zone of the hippocampus. Furthermore, moderate catch-up growth at the three time points improved memory function while maintaining a normal mPAP. In adult IUGR rats experiencing rapid catch-up growth, although memory function improved, elevated mPAP and medial thickening of pulmonary arterioles were observed. Additionally, PASMCs exhibited excessive proliferation, migration and anti-apoptotic activity in the rapid catch-up group, and PVECs also displayed excessive proliferation. These results suggested that moderate catch-up growth after IUGR is a better strategy for optimal cognition and cardiovascular health in adulthood compared with rapid catch-up growth or delayed growth.

Correspondence to: Professor Lizhong Du, Department of Neonatology, Children's Hospital, Zhejiang University School of Medicine, 3333 Binsheng Road, Hangzhou, Zhejiang 310052, P.R. China
E-mail: dulizhong@zju.edu.cn

Key words: intrauterine growth restriction, catch-up growth, cognitive function, pulmonary arterial hypertension, smooth muscle cells, endothelial cells

Introduction

Intrauterine growth restriction (IUGR) is defined as a reduced rate of fetal growth compared with the growth potential of a specific infant based on their ethnicity and sex (1). Genetic factors, fetal factors, placental issues or maternal health issues can all lead to the occurrence of IUGR (2,3). IUGR is one of the leading causes of perinatal-neonatal morbidity and mortality (4), which also carries long-term consequences (5). Notably, IUGR can result in significant neurological deficits (6), which can affect the development of the brain in offspring (7). In clinical practice, to prioritize the development of the brain, a catch-up growth pattern is recommended to facilitate a swift recovery to a normal growth trajectory for infants with IUGR (8-10).

Rapid catch-up growth promotes development but also presents numerous potential problems. For individuals with IUGR, postnatal catch-up growth can help them achieve a normal weight, height, head circumference and neurodevelopment; however, adverse consequences of catch-up growth have been identified, including abnormal gut microbiota (8), cardiovascular disease (11), insulin resistance (12) and obesity (13). Our previous research showed that while postnatal rapid catch-up growth in IUGR rats can increase pulmonary artery pressure (PAP) in adulthood, postnatal delayed growth reduces the risk of pulmonary vascular dysfunction but has long-term negative effects on cognitive function (14). Determining whether to provide adequate nutrition for infants with IUGR to achieve catch-up growth, and to what extent catch-up growth should be pursued remains challenging.

Offspring with IUGR have a higher susceptibility to elevated PAP in adulthood compared with offspring that receive adequate intrauterine nutrition (15,16). A randomized

controlled trial indicated that catch-up growth in early postnatal life, rather than simply being born with IUGR, poses a risk for developing cardiovascular diseases later in adulthood (17). This result emphasizes the significance of early postnatal growth patterns in children with IUGR. A systematic review by Kelishadi *et al* (18) also supported this viewpoint, stating that rapid postnatal catch-up growth of low birthweight neonates is a more important factor than low birthweight alone in cardiovascular disease and its risk factors. Furthermore, animal experiments have demonstrated that IUGR is associated with the development of pulmonary arterial hypertension (PAH) in adulthood (19-21). PAH is characterized by excessive pulmonary vascular remodeling, which involves dysregulated proliferation of cells in the intima, media and adventitia (22). The pathological mechanisms underlying PAH include increased inflammation and proliferation, and reduced apoptosis of pulmonary artery smooth muscle cells (PASMCs) (23), as well as excessive proliferation and survival of pulmonary vascular endothelial cells (PVECs) (22). Based on the fact that postnatal rapid catch-up growth in IUGR rats may lead to elevated PAP in adulthood (14), it is worth exploring whether rapid catch-up growth in IUGR rats also leads to PAH-like pathophysiological development of smooth muscle cells and endothelial cells.

It is well known that excessive nutrition can lead to cardiovascular diseases, while malnutrition can impact brain development. In the case of infants with IUGR, there is currently no consensus on the optimal nutritional intervention strategies after birth, particularly regarding how to balance cardiovascular function and brain function in adulthood. 'Healthy catch-up growth' is a future research direction (10); a reasonable strategy to achieve this is to implement postnatal interventions with the aim of avoiding rapid catch-up growth by promoting moderate prolonged growth (24). In the present study, an IUGR model was established by restricting maternal nutrition during pregnancy and different postnatal growth patterns were achieved by adjusting the litter size during lactation. It was hypothesized that early moderate catch-up growth would preserve mean PAP (mPAP) in adult IUGR rats while not affecting the development of their memory function. The present study may provide valuable insights into further exploration of the mechanisms and effects of early postnatal nutritional interventions in human infants with IUGR.

Materials and methods

Ethics statement. All animal care and experiments were performed in strict accordance with the guidelines for the Care and Use of Laboratory Animals (25) and were approved by the Institutional Animal Care and Use Committee (IACUC) of Zhejiang University (Hangzhou, China; approval no. ZJU20160215). The extraction of primary PASMCs and primary PVECs from rat lungs for research purposes was also approved and permitted by the IACUC of Zhejiang University (approval no. ZJU20160215; Hangzhou, China). Sprague Dawley (SD) rats were obtained from the Animal Center of the Chinese Academy of Sciences (http://www.slaccas.com/; Shanghai, China). All surgical procedures were performed under anesthesia using sodium pentobarbital, and every effort was made to minimize pain and discomfort.

In the present study, humane endpoints were implemented to monitor the well-being of the animals and to ensure ethical treatment. These endpoints included assessing vital signs, body weight, behavior and other relevant indicators. In addition, the rats were closely observed for any signs of distress, pain or significant deterioration in health. If any animals reached the predefined endpoint criteria, such as severe weight loss (weight loss range, 20-25%), inability to eat or drink, or signs of severe illness, they were euthanized to minimize suffering. Euthanasia was performed by intraperitoneal injection of 200 mg/kg sodium pentobarbital. These humane endpoints were established in accordance with ethical guidelines and were approved by the relevant animal welfare committee.

IUGR and catch-up growth animal model. The SD rats (total of 198; 99 males and 99 females; 9 weeks old) were housed in a specific pathogen-free environment, under an ambient temperature of 22±2˚C and ~60% humidity, with a 12-h light/dark cycle. As described previously, a rodent model of nutrient restriction during pregnancy was used to induce IUGR in the offspring (14,19,26). When virgin female SD rats reached a weight of 250-300 g, they were mated overnight with male rats in a 1:1 ratio. The following day, vaginal smears were taken to confirm successful pregnancy by examining the presence of sperm, which was considered the first day of pregnancy. The pregnant rats (n=99) were randomly assigned to either a normal diet group (n=63) or a restricted diet group (n=36). The normal diet group was provided *ad libitum* access to food, whereas the restricted diet group was provided with 50% of the normal food amount. Both groups had free access to water. Each pregnant rat was housed in a cage until delivery and the offspring were weighed on the first day after birth. Each dam underwent only one reproductive cycle. The offspring of the normal diet group were labeled as the control pups, whereas those in the restricted diet group with birth weights below the 10th percentile of the control group (<6.665 g) were labeled as the IUGR pups. Rats with birth weights ≥10th percentile of the control group were euthanized by intraperitoneal injection of an overdose of 2% sodium pentobarbital (200 mg/kg). After birth, the litter size was adjusted and the pups were divided into four experimental groups. The control group was fed with a litter size of eight control offspring/litter. The IUGR pups were randomly assigned to three different feeding strategy groups, with litter sizes of 5, 10 or 16 pups/litter; these groups represented the rapid catch-up growth, moderate catch-up growth and delayed growth groups, respectively. All pups from the four groups were breastfed by dams with *ad libitum* access to food during pregnancy (15 dams were used to breastfeed the control pups, while the remaining 48 dams were used to breastfeed the IUGR pups). During the lactation period, the male-to-female ratio of pups in each litter was 1:1, except for the rapid catch-up growth group, which had a ratio of 3:2. IUGR rats with excessively low birth weights were prone to early postnatal mortality, and in this study, the mortality rate during the lactation period for IUGR rats was 30.3%; this rate is lower than that reported in a previous study (19), a difference that could be attributed to the birth weight of the IUGR rats and the rearing environment. If pup mortality occurred during lactation, an equal number of female rats born during the same period were added to maintain a consistent litter size.

Based on previous research, 3-week-old rats are equivalent to 2-year-old human infants (27). Additionally, it has been observed that most human SGA individuals exhibit catch-up growth within the first 2 years (8,9). Therefore, rats that achieved a weight ≥10th percentile (≥P10) of the control group at weaning (3 weeks) were deemed to have successfully achieved catch-up growth. After excluding rats whose weight did not meet the requirement (rats with a weight >90th percentile were considered overweight), rats were divided into two groups: Moderate catch-up growth and rapid catch-up growth. This division was based on the 50th percentile (P50), with ~50% of the rats meeting the weight criteria. In addition, rats with a weight <P10 of the normal group were classified as the delayed growth group, and all rats in this group met the weight criteria. When weaning the offspring at 3 weeks of age, the percentiles (P10, P50 and P90) of the body weight in the normal control group were calculated. Male IUGR rats that met the weight requirements for follow-up studies were used, whereas those that did not meet the weight requirements and female rats were euthanized via intraperitoneal injection of 2% sodium pentobarbital (200 mg/kg). Death was assessed when the rats exhibited a loss of pain response, showing no reaction to the manual pressure applied to their toes. Additionally, their pupils were fixed and dilated, and the absence of heartbeat and respiration was confirmed, along with a noticeable decrease in body temperature, conclusively indicating successful sacrifice.

As the weights of the IUGR rats obtained through different feeding methods did not all meet the experimental requirements, further selection was necessary at 3 weeks old. IUGR rats were divided into three subgroups based on their weight at the time of weaning (3 weeks): IUGR with rapid catch-up growth in early postnatal life (IUGR + RC, P50-P90), IUGR with moderate catch-up growth in early postnatal life (IUGR + MC, P10-P50, including P10 and P50), and IUGR with delayed growth in early postnatal life (IUGR + DG, <P10). Subsequently, all four groups of rats were provided *ad libitum* access to food and water until they reached 13 weeks of age, and their body weights were monitored on a weekly basis. Each cage contained four rats to mitigate the influence of housing density on body weight. The experiments were performed at three time points: 3, 9 and 13 weeks. Each group at each time point consisted of 20-22 eligible offspring rats, which were used for subsequent experiments. To eliminate the variation caused by the hormonal cycle of female rats, only male rats were used in subsequent experiments.

During the lactation period, the health and behavior of the animals were monitored daily, ensuring a consistent number of pups per litter. After weaning at 3 weeks, the animal health and behavior was assessed once a week and their weights were recorded. In the present study, no rats reached any of the humane endpoints, such as severe weight loss, inability to eat or drink, or signs of severe illness.

Y-maze test for spontaneous alternation. The Y-maze spontaneous alternation test is used to assess spatial working memory in rats by allowing them to freely explore the three arms of a maze (28,29). This behavior is driven by the innate curiosity of rodents to explore areas they have not previously visited. The apparatus consists of three identical black arms, each at a 120° angle, 50 cm in length, 35 cm in height and 18 cm in width. Three spontaneous alternation tests at 3, 9 and 13 weeks of age were performed to evaluate the working memory of rats at the different stages of development (n=20-22/group). The rats were placed at the end of one arm of the Y-maze, with their backs to the center, and allowed to freely explore for 8 min. A camera positioned above the center of the maze captured the movement trajectory of the rats throughout the maze. The ANY-maze version 7.0 software (Stoelting Co.) was used to analyze the percentage of alternation, total number of arm entries and total distance traveled in the maze. The percentage of alternation was calculated using the following formula (30,31): Alternation (%)=(number of alternations/total arm entries-2) x100.

Hemodynamic and right ventricular hypertrophy assessment. An open-chest surgical procedure was used to assess the right ventricular system in 3-week-old rats. Due to their small body size, the mean abdominal aortic pressure (mAAP) of the rats was not measured. For 9- and 13-week-old rats, closed-chest surgery was used to measure their PAP.

For 3-week-old rats, as described in our previous study (32), the rats were anesthetized with 2% sodium pentobarbital (50 mg/kg, intraperitoneal injection) and fixed on a temperature-controlled surgical table (37°C) after weaning. The fur on the chest and neck was removed, and the chest and neck area was disinfected with 75% alcohol. Subsequently, the skin was cut to expose the trachea. The tracheal intubation catheter was connected to a small animal ventilator, and the respiratory rate and tidal volume were calculated and adjusted based on weight (33). After a few minutes of stable breathing, the right third and fourth intercostal spaces were carefully separated to expose the right ventricle (RV). A heparinized saline infusion needle (0.45x13.5 mm) was inserted vertically into the RV, and the other end was connected to a pressure sensor. The physiological data acquisition system (Biopac Systems, Inc.) recorded the hemodynamic parameters. The PAP value was indirectly reflected by the right ventricular systolic pressure. Additionally, the mean right ventricular pressure (mRVP) was recorded. After measurement, the rats were euthanized by exsanguination through the abdominal aorta, and the heart and lungs were exposed. Subsequently, 0.9% cold saline was injected into the left ventricle (LV) until the liver turned yellow; this is a commonly used method to ensure thorough perfusion of the brain and lungs. The perfused brain (white) and lungs (white) were collected for subsequent morphometric analysis. The heart was completely removed, including the left and right atria, as well as the free large vessels. The right ventricular wall was cut along the interventricular septum (S). To assess the extent of right ventricular hypertrophy, the weights of the RV, LV and S were measured. The right ventricular hypertrophy index (RVHI) was then calculated using the following formula: RVHI=RV/(LV + S).

For the 9- and 13-week-old rats, a closed-chest surgical method was performed to measure their PAP (19). After anesthesia using 2% sodium pentobarbital (50 mg/kg, intraperitoneal injection), the rats were immersed in 75% alcohol for disinfection, then the fur on their neck and abdomen was removed. They were then placed on a temperature-regulated surgical table set at 37°C. A PE-50 catheter filled with heparin saline was connected to a pressure sensor at one end and

inserted through the right jugular vein into the RV, and finally into the pulmonary artery. The position of the catheter was determined based on the waveform measured by the physiological data acquisition system (Biopac Systems, Inc.). After the waveform stabilized, hemodynamic values were measured for 2-3 min. Then, the catheter was removed, and pressure was applied with a cotton ball to stop bleeding. The abdominal cavity was then opened, and the abdominal aorta was fully exposed. After flushing the catheter with heparin saline, it was inserted into the abdominal aorta to measure the mean mAAP. After measuring, the rats were euthanized by exsanguination through the abdominal aorta, and the heart and lungs were exposed. A total of 10 ml 0.9% cold physiological saline was injected into the RV and perfused through the pulmonary artery to the entire lung. The perfused lungs (appearing white) were collected for subsequent extraction of PASMCs, PVECs, western blotting and morphometric analysis. The same steps as aforementioned were used to calculate RVHI. In addition, the ratio of pulmonary and systemic circulation pressure was calculated as Pp/Ps. No rats died during anesthesia or surgical procedures in the present study.

Quantitative analysis of neural stem cell numbers in the hippocampus. Double immunofluorescence staining of hippocampal tissue was used to investigate neurogenesis in the dentate gyrus. The isolated brain tissue was fixed overnight at 4˚C in 4% paraformaldehyde, dehydrated through a graded series of alcohols, and then embedded in paraffin to form paraffin blocks, and cut into 5-μm thick paraffin-embedded sections. Brain paraffin-embedded sections were subjected to dewaxing, hydration, high-temperature antigen retrieval using sodium citrate antigen retrieval solution at 100˚C for 20 min (cat. no. P0081; Beyotime Institute of Biotechnology) and blocking in 5% BSA containing 0.5% Triton X-100 at 37˚C for 30 min (cat. no. ST025-5g; Beyotime Institute of Biotechnology). The sections were then incubated overnight at 4˚C with the following primary antibodies: Anti-NeuN (1:200; cat. no. ab104224; Abcam) and anti-Ki67 (1:100; cat. no. ab16667; Abcam). Subsequently, fluorescent secondary antibodies were incubated with the sections in the dark for 1 h at 37˚C: Goat anti-mouse Alexa Fluor® 594 (1:1,000; cat. no. ab150116; Abcam) and goat anti-rabbit Alexa Fluor 488 (1:1,000; cat. no. ab150077; Abcam). The nuclei were counterstained with DAPI in the dark at room temperature for 7 min and the sections were observed under a fluorescence microscope (Carl Zeiss AG). The number of Ki67-positive cells in the subgranular zone (SGZ) of the dentate gyrus was counted, and considered the number of neural stem cells.

Hematoxylin and eosin (H&E) staining. H&E staining was used to evaluate pulmonary vascular remodeling. The lung tissues perfused in each group were fixed in 4% paraformaldehyde for 24 h. They were then subjected to alcohol gradient dehydration, paraffin embedding and sectioning into 5-μm thick slices. The sections were stained according to the instructions provided in the H&E Staining Kit (cat. no. C0105S; Beyotime Institute of Biotechnology), and finally sealed with a neutral resin. The morphology of rat lung blood vessels was observed using a light microscope. Small arteries (diameter, 20-100 μm) were selected for analysis. ImageJ (version 1.8.0; National Institutes of Health) was used to analyze the percentage of vascular medial wall thickness (WT%). This was calculated using the following formula: WT%=(outer diameter-inner diameter)/outer diameter x100.

Immunohistochemical staining. Rat lung tissues embedded in paraffin were sectioned into 5-μm sections. Lung tissue sections were baked at 62˚C for 1 h, followed by deparaffinization in xylene and rehydration in a descending ethanol series. Then, the sections were treated at 100˚C for 20 min in citrate antigen retrieval solution (cat. no. P0081; Beyotime Institute of Biotechnology). After cooling, the sections were incubated at room temperature in 3% hydrogen peroxide for 20 min to block endogenous peroxidase activity. Subsequently, the sections were incubated at 37˚C for 30 min in 5% BSA (cat. no. ST025-5g; Beyotime Institute of Biotechnology) for blocking. After blocking, the sections were incubated overnight at 4˚C with diluted α-SMA antibody (1:400; cat. no. 19245s; Cell Signaling Technology, Inc.). The next day, the sections were incubated for 2 h at 37˚C with goat anti-rabbit IgG H&L (HRP) secondary antibody (1:1,000; cat. no. ab6721; Abcam). Color development was performed using the DAB Horseradish Peroxidase Color Development Kit (cat. no. P0203; Beyotime Institute of Biotechnology) according to the instruction manual. Images were captured under white light using an optical microscope and analyzed with ImageJ (version 1.8.0 software; National Institutes of Health). Immunohistochemical staining was conducted to detect the expression of α-SMA in the pulmonary arterioles at three different time points, further evaluating the degree of pulmonary vascular muscularization in the 13-week-old rats. The area and outer circumference of α-SMA positive staining (yellow) in pulmonary arterioles (diameter, 20-100 μm) were measured and calculated using ImageJ. The ratio was calculated to evaluate the thickness of the vascular medial layer, with a higher ratio indicating a thicker pulmonary vascular medial layer. Quantitative analysis of the number of alveolar ducts and vascular alveolar walls in 13-week-old rats was performed using a light microscope. Each vessel was categorized as muscular, partially muscular or non-muscular. A total of 30 vessels were counted per rat. The number and degree of muscularization of these arteries were quantitatively analyzed as described previously (34,35).

Primary PASMCs culture and identification. PASMCs were extracted from the lungs of 9- and 13-week-old rats in a laminar flow hood, using sterile techniques. As described previously (36), the pulmonary artery was isolated, and the adventitia and endothelium were carefully scraped off. The pulmonary blood vessels were washed three times in sterile PBS then placed into a smooth muscle digestion solution (papain and collagenase dissolved in PBS; Sigma-Aldrich; Merch KGaA), cut into ~1 mm^3 pieces using ophthalmic scissors, and subsequently digested in a constant temperature water bath at 37˚C for 30 min. After completing the digestion, the samples were centrifuged at 1,000 x g for 5 min at room temperature. The supernatant was discarded, the sedimented tissues were combined with 3 ml high-glucose DMEM (cat. no. CR-12800-S; Zhejiang Senrui Biotechnology Co., Ltd.) supplemented with 15% FBS (cat. no. 10099-141C, Gibco; Thermo Fisher Scientific, Inc.) and 1% penicillin-streptomycin.

The mixture was then evenly distributed at the bottom of a 25-cm^2 culture flask. After 3 days of culturing, the medium was replaced with fresh medium. After 5 days, cells began to grow out from the tissue samples. The medium was replaced with fresh medium every 2 days thereafter. When the cells reached 80% confluence, they were passaged using 0.25% trypsin (Gibco; Thermo Fisher Scientific, Inc.). Cell morphology was observed under a bright-field microscope, and PASMCs were identified by immunofluorescent staining using an α-SMA antibody (1:400; cat. no. 19245s; Cell Signaling Technology, Inc.), with a cell purity of >90%. Subsequent studies were conducted using PASMCs from passages 2-4.

Primary PVECs culture and identification. According to our previous study (19), primary PVECs were extracted from 13-week-old rats. Briefly, the lungs were perfused and washed with ice-cold sterile PBS. A 2 mm-wide strip was cut along the edge of the lung and sliced into 3-5 mm pieces, and strips were evenly spread in a 75 cm^2 culture flask. The flask was filled with endothelial cell-specific culture medium (5% FBS, 1% endothelial cell growth supplement and 1% penicillin-streptomycin; ScienCell Research Laboratories, Inc.). Additionally, the medium was supplemented with 90 U/ml heparin (cat. no. H3149; Sigma-Aldrich; Merch KGaA) to inhibit fibroblast growth and purify endothelial cells. On day 2, the medium was replaced with fresh endothelial cell culture medium, and on day 5, tissue blocks were removed by tapping the culture flask. When the confluence of endothelial cells reached ~80%, cell morphology was observed under a light microscope. PVECs were then identified by immunofluorescent staining using a CD31 antibody (1:100; cat. no. ab24590; Abcam), with a cell purity of >90%. Subsequent studies were conducted using PVECs from passages 1-2.

Immunofluorescence staining. Primary PASMCs or PVECs, cultured in 24-well plates, were fixed with 4% paraformaldehyde on ice for 30 min. They were then blocked with a solution of 3% BSA and 0.5% Triton X-100 dissolved in PBS for 1 h at 37˚C. The cells were then incubated with α-SMA (1:400; cat. no. 19245s; Cell Signaling Technology, Inc.) or CD31 (1:100; cat. no. ab222783; Abcam) primary antibodies overnight at 4˚C. The following day, the cells were incubated with the following secondary antibodies for 1 h at 37˚C in the dark: Goat anti-rabbit Alexa Fluor 488 (1:1,000; cat. no. ab150077; Abcam) or goat anti-mouse Alexa Fluor 488 (1:1,000; cat. no. ab150113; Abcam). Then, the nuclei were labeled with DAPI for 7 min at room temperature. All images were observed under a fluorescence microscope (Carl Zeiss AG).

EdU cell proliferation assay. Cell proliferation was detected using an EdU Cell Proliferation Assay Kit (Apollo®567; Guangzhou RiboBio Co., Ltd.) according to the manufacturer's instructions. PASMCs or PVECs ($1x10^5$ cells/ml) cultured in a 96-well plate were incubated with 50 μM EdU for 2 h at 37˚C, and then the medium was discarded. After fixing with 4% paraformaldehyde at room temperature for 30 min, and permeabilizing with 0.5% Triton X-100 for 10 min at room temperature, 100 μl 1X Apollo staining reaction solution was added to each well and incubated at room temperature in the dark for 30 min. Cells were then stained with 1X Hoechst 33342 for 30 min at room temperature to visualize the cell nuclei, and cell counting was performed using an inverted fluorescence microscope (Carl Zeiss AG). To quantify the proliferation rate of PASMCs or PVECs, the relative EdU-positive ratio was calculated by randomly selecting six visual fields from each sample image.

Transwell assay. A Transwell assay was used to evaluate the migratory ability of PASMCs. Transwell chambers (24-well plate; pore size, 8.0 μm; Corning, Inc.) coated with Matrigel Basement Membrane Matrix (diluted 1:15 in DMEM; cat. no. 354234; Corning, Inc.) and incubated for 2 h at 37˚C before use. After the Matrigel dried, the chamber was placed in a 24-well plate. Primary PASMCs were resuspended in serum-free DMEM and seeded in the upper chamber, whereas DMEM containing 10% FBS was loaded into the lower chamber. After incubating at 37˚C for 48 h, the cells on the membrane surface were carefully removed. The PASMCs that had migrated to the underside of the membrane were then fixed with 4% paraformaldehyde at room temperature for 20 min and stained with 0.1% crystal violet (Beyotime Institute of Biotechnology) at room temperature for 20 min. Images were obtained using an optical microscope (Carl Zeiss AG), and the number of cells that had migrated through the membrane was counted using ImageJ.

TUNEL staining. PASMCs were in a proliferative state in conventional complete culture medium (high-glucose DMEM supplemented with 15% FBS and 1% penicillin-streptomycin), with low levels of apoptosis. To investigate the anti-apoptotic activity of PASMCs, the cells were cultured in DMEM supplemented with 0.1% FBS for 48 h. This use of a low serum concentration creates a 'hunger' condition that induces apoptosis (37). According to our previous study (19), the one-step TUNEL Cell Apoptosis Detection Kit (cat. no. C1086; Beyotime Institute of Biotechnology) was used to detect the apoptotic rate of PASMCs. All images were observed under a fluorescence microscope (Carl Zeiss AG). To quantify the apoptotic rate of PASMCs, the relative ratio of FITC-labeled (green) positive cells was calculated by randomly selecting six visual fields from each sample image.

Western blotting. The perfused, clean lung tissues and collected PASMCs were stored at -80˚C for future use. Total protein was extracted from lung tissues and PASMCs for western blot analysis to investigate differences in the protein expression levels between the groups. The specific steps have been described previously (38). After blocking the membranes with 5% milk at room temperature for 1 h, they were incubated with the following primary antibodies overnight at 4˚C: α-SMA (1:1,000; cat. no. 19245s; Cell Signaling Technology, Inc.), endothelial nitric oxide synthase (eNOS; 1:1,000; cat. no. ab199956; Abcam), inducible NOS (iNOS; 1:1,000; cat. no. 18985-1-AP; ProteinTech Group, Inc.), Bcl-2 (1:1,000; cat. no. 26593-1-AP; ProteinTech Group, Inc.), Bax (1:1,000; cat. no ET1603-34; Huabio), cleaved caspase-3 (1:1,000; cat. no. 9664s; Cell Signaling Technology, Inc.), caspase-3 (1:1,000; cat. no. 9662s; Cell Signaling Technology, Inc.), Ki67 (1:100; cat. no. ab16667; Abcam) or β-actin (1:10,000; cat. no. 8457s; Cell Signaling Technology, Inc.). The following day,

a HRP-linked secondary antibody (goat anti-rabbit; 1:3,000; cat. no. 7074; Cell Signaling Technology, Inc.) was used to incubate the membranes at room temperature for 2 h. The ECL chemiluminescent developing solution (cat. no. WBKLS0050; Sigma-Aldrich) was prepared at a 1:1 ratio and shielded from light. After the addition of the developing solution, the bands were detected using the G: BOX gel doc system (Syngene). All bands were generated on a single PVDF membrane (IPVH00010/ISEQ00010; MilliporeSigma). For examination of proteins with similar molecular weights, membranes were stripped using a stripping buffer (cat. no. 46430; Thermo Fisher Scientific, Inc.), and after blocking with 5% milk for 1 h, the membrane was incubated with the next primary and secondary antibodies as aforementioned. Protein expression was semi-quantified by normalizing to the relative β-actin expression using ImageJ.

Statistical analysis. All experiments were repeated three times. Statistical analyses were performed using SPSS version 20.0 (IBM Corp.) and GraphPad Prism version 8.3.0 (Dotmatics). One-way ANOVA followed by Tukey's post hoc test was used to analyze the differences between more than two groups. Independent samples between two groups were analyzed using an unpaired Student's t-test. Data are presented as the mean ± SEM. $P<0.05$ was considered to indicate a statistically significant difference.

Results

Establishment of three different growth patterns in early postnatal life and weight analysis of IUGR rats. The IUGR model was established by restricting maternal nutrition during pregnancy, and different postnatal growth patterns were constructed by adjusting the number of pups in each group during lactation (Fig. 1A). The offspring of dams with restricted maternal nutrition had birth weights <P10 (6.665 g) of the control group (4.70±0.06 g vs. 7.22±0.11 g; Fig. 1B), indicating the successful establishment of the IUGR model. These IUGR rats were randomly assigned to be nursed by dams on a normal diet during lactation, with litter sizes of 5, 10 or 16 pups per dam. There were no differences in the birth weight among the three IUGR groups with different growth patterns (Fig. 1C). In addition, the weight curve indicated that there were no significant differences in the weights between the IUGR + RC group and the control group at weaning (3 weeks). The weight curve of the IUGR + MC group remained between that of the IUGR + RC and the IUGR + DG groups throughout the study. Notably, the weight of the IUGR + DG group was lower than that of the control group at all time points (Fig. 1D). These results indicated that, compared with the IUGR + DG group, the rats in the two other catch-up growth groups demonstrated improved growth and development.

Postnatal catch-up growth in IUGR rats can improve memory function deficits. The Y-maze was used to assess short-term memory in rats. The spontaneous alternation test was performed on rats at 3, 9 and 13 weeks of age, and the movement trajectory of the rats in the Y-maze was recorded (Fig. 2A, C and E). Quantitative analysis showed that the percentage of spontaneous alternations in the IUGR + DG group was significantly lower than that in the control group at all three time points (Fig. 2B, D and F). In addition, there was no significant difference in the total number of arm entries and total distance traveled in the maze among the groups at the three time points.

Neurogenesis in the dentate gyrus of the hippocampus was investigated in 3-week-old rats using double immunofluorescence staining for NeuN and Ki67 (Fig. 2G). The number of Ki67-positive cells in the SGZ in the IUGR + DG group was significantly lower than that in the other three groups (Fig. 2H). These results indicated that delayed growth after IUGR led to a decrease in the number of proliferating neurons in the SGZ, resulting in a decrease in spatial working memory in rats. However, postnatal catch-up growth, whether it was moderate or rapid, could improve memory function deficits in IUGR rats during both childhood and adulthood.

Moderate postnatal catch-up growth in IUGR rats preserves normal PAP in adulthood. Subsequently, the effects of the three different growth patterns on PAP and RVP were investigated through invasive hemodynamic analysis. The results showed that at 3 (Fig. 3A and B) and 9 weeks of age (Fig. 3C and D), there were no significant differences in mPAP, mRVP and RVHI between the control and the IUGR + RC group. However, at 13 weeks of age, the mPAP of the IUGR + RC group was significantly higher than that of the control group (18.37±0.18 mmHg vs. 21.1±0.44 mmHg; Fig. 3E and F). In addition, the mPAP of the IUGR + MC group (19.25±0.20 mmHg) and the IUGR + DG group (18.64±0.23 mmHg) were significantly lower than that of the IUGR + RC group. There were no signficant differences in the mRVP and RVHI among the groups at 13 weeks of age. Next, the systemic circulation pressure of rats was evaluated by measuring the mAAP (Fig. 3G). At 9 weeks of age, no significant differences were observed in mAAP and Pp/Ps among the four groups of rats (Fig. 3H). At 13 weeks of age, although mAAP remained similar, the Pp/Ps of the IUGR + RC group was higher than that of the control group (Fig. 3I). This further demonstrated that rapid catch-up growth led to an increase in pulmonary circulation pressure in adult IUGR rats, but did not affect systemic circulation pressure. Moderate catch-up growth and delayed growth did not have a marked impact on PAP and RVP in adult rats. These results indicated that compared with the other two growth patterns, early moderate catch-up growth following IUGR led to better memory and pulmonary vascular function in adulthood.

Moderate postnatal catch-up growth prevents pulmonary arteriolar remodeling compared with rapid catch-up growth. Due to the observation that postnatal rapid catch-up growth increased PAP in adulthood, whether it also affected pulmonary arteriolar remodeling was assessed. To test this hypothesis, H&E staining was used to observe lung small artery structure in rats at 3, 9 and 13 weeks of age in the different groups (Fig. 4A). No significant differences were observed in WT% among the groups at 3 and 9 weeks of age. At 13 weeks, the IUGR + RC group showed a significant increase in medial WT% compared with that in the

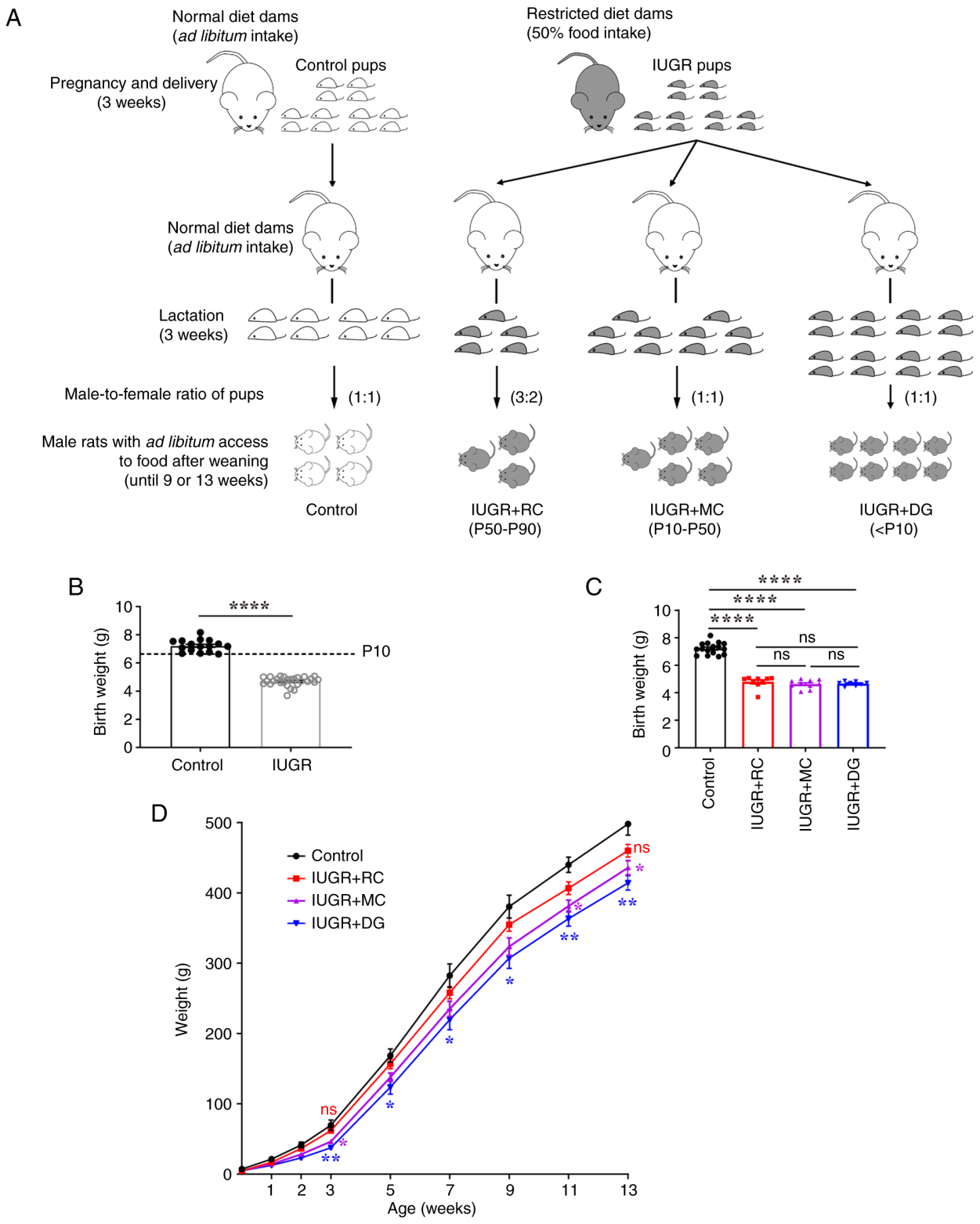

Figure 1. Preparation of the animal model and body weight curve of rats in each group. (A) Schematic diagram of the generation of IUGR and different postnatal growth pattern models. (B) Birth weights of pups (Control, n=16; IUGR, n=27). Data were analyzed using Student's two-tailed t-test. (C) Birth weight of the four groups of rats (Control, n=16; IUGR + RC, n=9; IUGR + MC, n=10; IUGR + DG, n=8). (D) Weight curve of rats from birth to 13 weeks of age (n=8-16/group). *P<0.05, **P<0.01, and ns vs. the control group. Data were analyzed using one-way ANOVA followed by Tukey's post hoc test. Data are presented as the mean ± SEM. *P<0.05, **P<0.01, ****P<0.0001. ns, not significant; IUGR, intrauterine growth restriction; RC, rapid postnatal catch-up growth; MC, moderate postnatal catch-up growth; DG, delayed growth in early postnatal life; P, percentile.

control group (29.06±1.32% vs. 55.16±4.75%; Fig. 4B). The IUGR + MC and IUGR + DG groups showed a marked decrease in WT% compared with that in the IUGR + RC group (Fig. 4B). Subsequently, the thickness of the medial smooth muscle layer and muscularization of lung small vessels were evaluated using α-SMA immunohistochemical

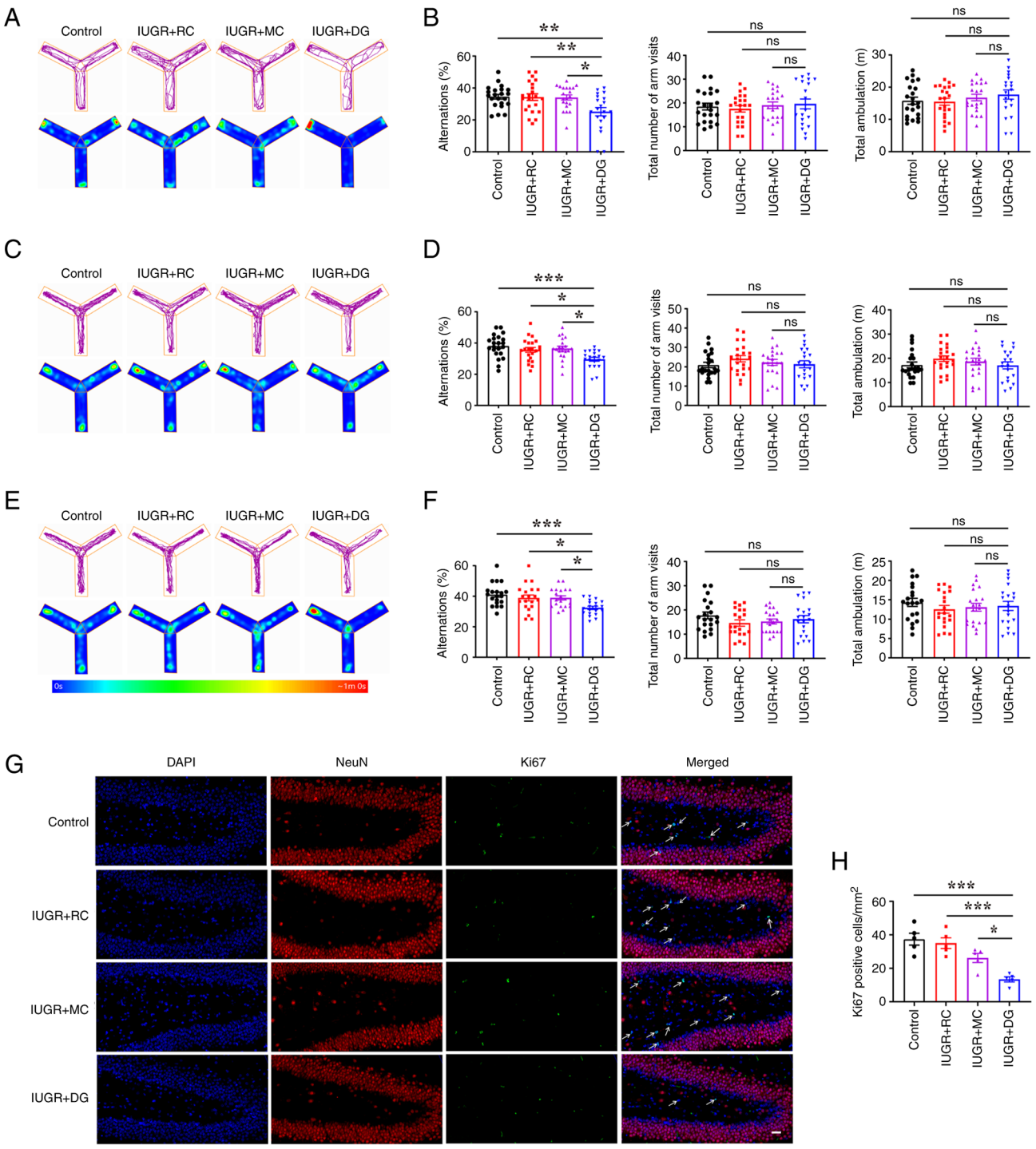

Figure 2. Effects of different growth modes on memory function and hippocampal neurogenesis after IUGR. (A) Representative Y-maze track of 3-week-old rats. (B) Quantitative analysis of alternation percentage, total arm entries and total maze running distance of 3-week-old rats (n=20-22/group). (C) Representative Y-maze track and (D) quantitative analysis of 9-week-old rats (n=20-22/group). (E) Representative Y-maze track and (F) quantitative analysis of 13-week-old rats (n=20/group). (G) Representative dual immunofluorescence staining of NeuN and Ki67 in the dentate gyrus area of 3-week-old rat hippocampus tissues. The white arrows show the Ki67-positive cells in the SGZ. (H) Statistical analysis of Ki67-positive cells in the SGZ area of the hippocampus (n=5/group). Data were analyzed using one-way ANOVA followed by Tukey's post hoc test. Data are presented as the mean ± SEM. *P<0.05, **P<0.01, ***P<0.001. ns, not significant; IUGR, intrauterine growth restriction; RC, rapid postnatal catch-up growth; MC, moderate postnatal catch-up growth; DG, delayed growth in early postnatal life; SGZ, subgranular zone.

staining (Fig. 4C-F). The results showed that at 13 weeks of age, compared with the control group, the IUGR + RC group exhibited significantly increased medial smooth muscle layer thickness (Fig. 4D) and percentage of muscular vessels (15.53±3.99% vs. 48.9±4.02%; Fig. 4E and F). Expression levels of α-SMA were also upregulated only in the IUGR + RC group compared with the control group (Fig. 4G and H). However, compared with in the IUGR + RC group, the IUGR + MC and the IUGR + DG groups exhibited a marked decrease in the thickness of the medial smooth muscle layer,

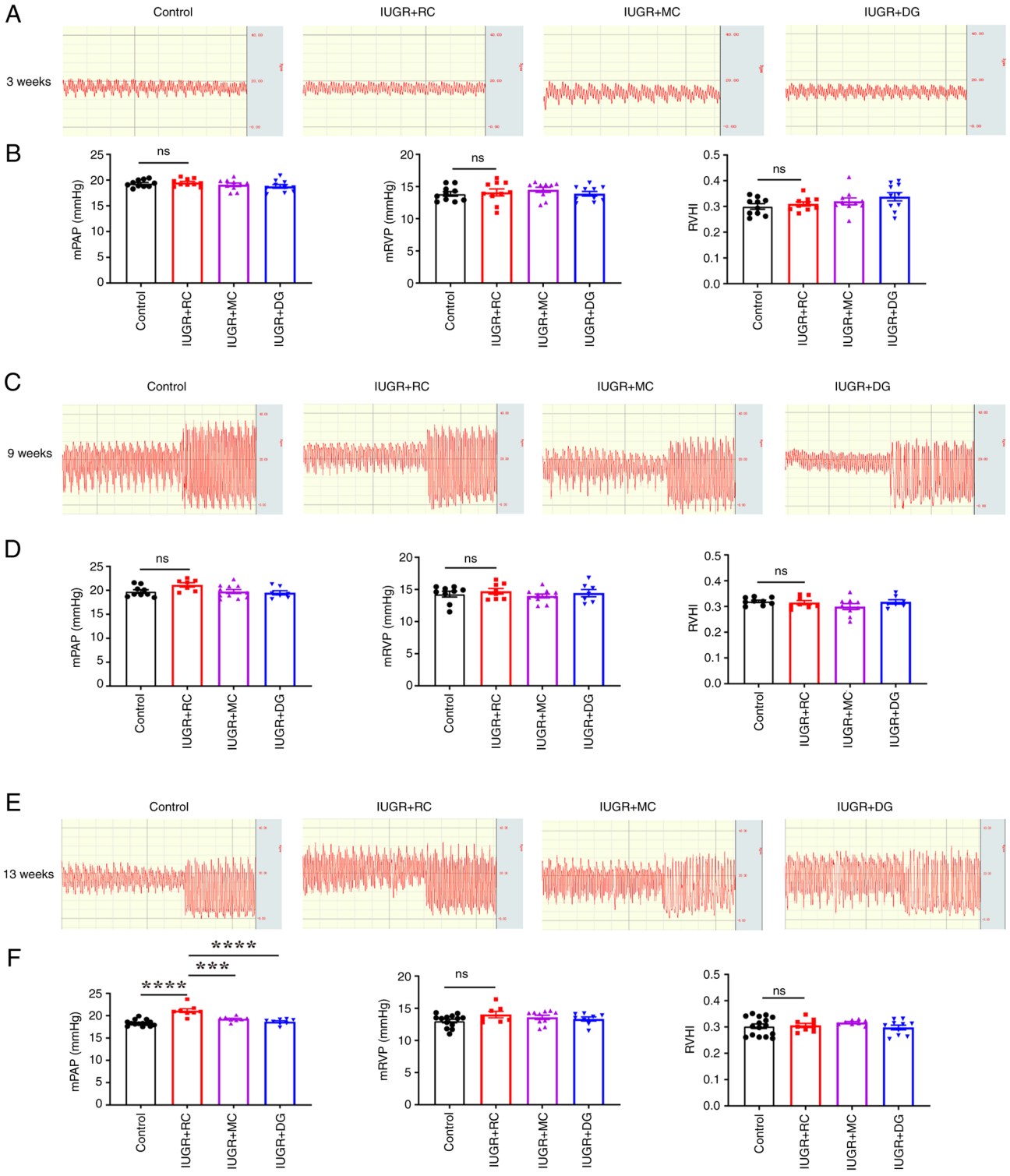

Figure 3. Continued.

the percentage of muscularized small blood vessels, and the expression of α-SMA at 13 weeks of age (Fig. 4E-H). Additionally, there was an increase in the percentage of non-muscularized blood vessels in the IUGR + MC and IUGR + DG groups compared with that in the IUGR + RC group (Fig. 4E and F). These results suggested that moderate catch-up growth had a minimal impact on pulmonary arteriolar remodeling, thus not leading to a significant elevation of PAP in adulthood.

Rapid catch-up growth downregulates the expression levels of eNOS, iNOS and apoptotic proteins in the lungs of adult IUGR rats. To further explore the molecular mechanisms underlying the increased PAP caused by rapid catch-up growth, western blotting was performed to analyze the protein expression levels in the lung tissue of adult rats from each group. The protein expression levels of eNOS and iNOS were assessed, and it was revealed that the IUGR + RC group exhibited decreased expression levels compared with those in the control group,

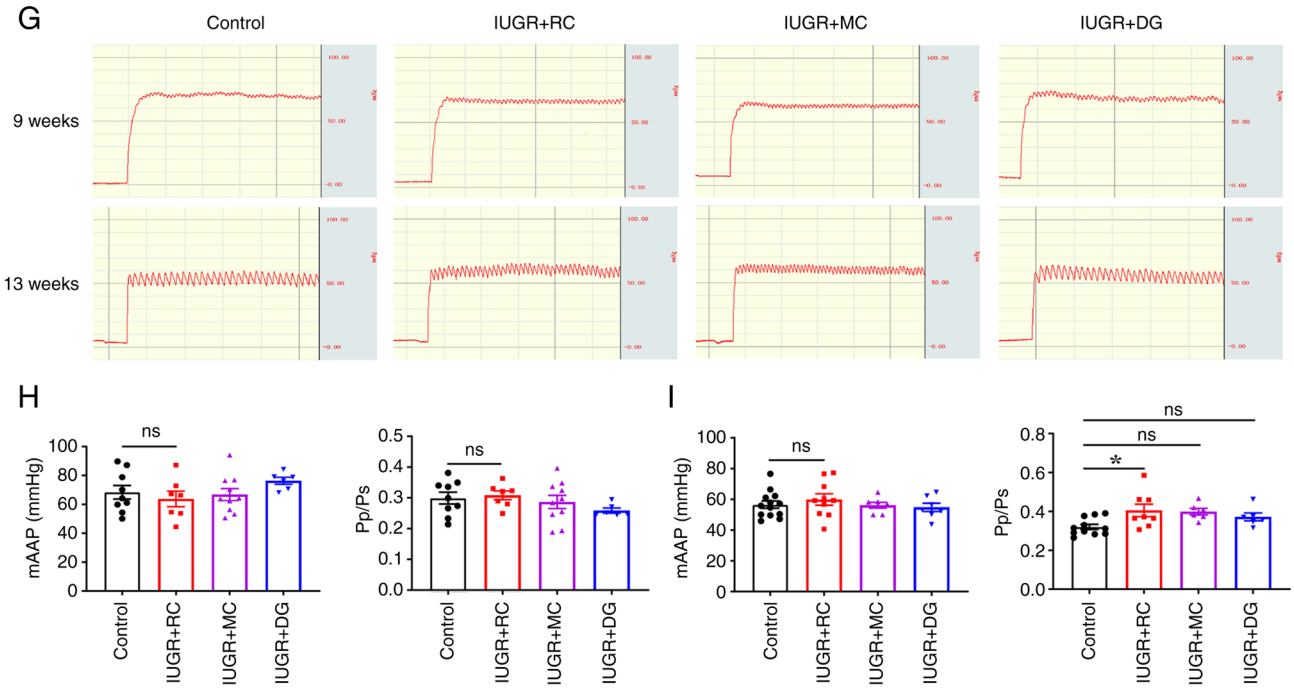

Figure 3. Moderate catch-up growth does not lead to increased PAP in adult IUGR rats. (A) Representative graphs of PAP in rats at 3 weeks of age. (B) Quantitative analysis of mPAP, mRVP and RVHI in 3-week-old rats (n=10/group). (C) Representative graphs of PAP in rats at 9 weeks of age. (D) Quantitative analysis of mPAP (n=7-11/group), mRVP (n=7-11/group) and RVHI (n=7-9/group) in 9-week-old rats. (E) Representative graphs of PAP in rats at 13 weeks of age. (F) Quantitative analysis of mPAP (n=8-14/group), mRVP (n=8-13/group) and RVHI (n=8-16/group) in 13-week-old rats. (G) Representative graphs of abdominal aortic pressure in rats at 9 and 13 weeks of age. (H) Quantitative analysis of mAAP (n=6-10/group) and Pp/Ps (n=6-10/group) in 9-week-old rats. (I) Quantitative analysis of mAAP (n=7-13/group) and Pp/Ps (n=7-13/group) in 13-week-old rats. Data were analyzed using one-way ANOVA followed by Tukey's post hoc test. Data are presented as the mean ± SEM. *P<0.05, ***P<0.001, ****P<0.0001. ns, not significant; IUGR, intrauterine growth restriction; RC, rapid postnatal catch-up growth; MC, moderate postnatal catch-up growth; DG, delayed growth in early postnatal life; mPAP, mean pulmonary artery pressure; mRVP, mean right ventricular pressure; RVHI, right ventricular hypertrophy index; Pp/Ps, ratio of pulmonary and systemic circulation pressure.

whereas the IUGR + MC group exhibited expression levels similar to those in the control group (Fig. 4I and J).

The expression levels of apoptosis-related proteins in the lungs were also assessed. The results showed that the IUGR + RC group exhibited increased expression levels of the anti-apoptotic protein Bcl-2, and decreased expression levels of the pro-apoptotic proteins Bax and cleaved caspase-3, whereas the IUGR + MC and the IUGR + DG groups did not exhibit significant differences compared with the control group (Fig. 4K and L). It was hypothesized that the increase in anti-apoptotic proteins in the IUGR + RC group may be associated with resistance to apoptosis in PASMCs. This was further supported by the increased ratio of total caspase-3 to cleaved caspase-3, indicating a potential suppression of apoptosis (Fig. 4L). In summary, these results indicated that postnatal rapid catch-up growth in IUGR may lead to a decrease in levels of pulmonary NOS, potentially resulting in reduced production of the vasodilator substance, NO. This, in turn, could have contributed to the elevation of PAP in adulthood.

Moderate catch-up growth prevents excessive proliferation, migration and anti-apoptotic effects of PASMCs compared with rapid catch-up growth. To gain a deeper understanding of the cellular mechanisms underlying pulmonary arteriolar remodeling in IUGR rats with postnatal rapid catch-up growth, primary PASMCs were cultured and cell identification assays were performed. Under an optical microscope, most primary rat PASMCs appeared as elongated spindle shapes with branching projections. Immunofluorescence staining for α-SMA showed a cell purity of ~91.3% (Fig. 5A), indicating successful isolation and cultivation of primary PASMCs. Next, the migration and proliferation of the primary PASMCs extracted from 9- and 13-week-old rats were evaluated. The results showed that there was no evident difference in the migratory and proliferative abilities of PASMCs among the groups at 9 weeks of age (Fig. 5B-E). However, at 13 weeks of age, the IUGR + RC group exhibited significantly increased migration (Fig. 5F and H) and a greater percentage of EdU-positive proliferating cells compared with those in the control group (Fig. 5G and I). The expression levels of Ki67 in the IUGR + RC group were also significantly higher than those in the control group (Fig. 5J-M).

Next, changes in apoptosis-related proteins in PASMCs extracted from the lungs of 13-week-old rats were evaluated using western blotting. The results showed that the expression levels of Bcl-2 were significantly upregulated, whereas the expression levels of Bax and cleaved caspase-3 were significantly downregulated in the IUGR + RC group compared with those in the control group (Fig. 6A). The increased ratio of total caspase-3 to cleaved caspase-3 further confirmed the apoptotic resistance in the PASMCs of the IUGR + RC group (Fig. 6A). TUNEL staining showed that PASMCs in the IUGR + RC group were more resistant to apoptosis induced by serum deprivation compared with that in the control group. By contrast, PASMCs in the IUGR + MC and IUGR + DG groups

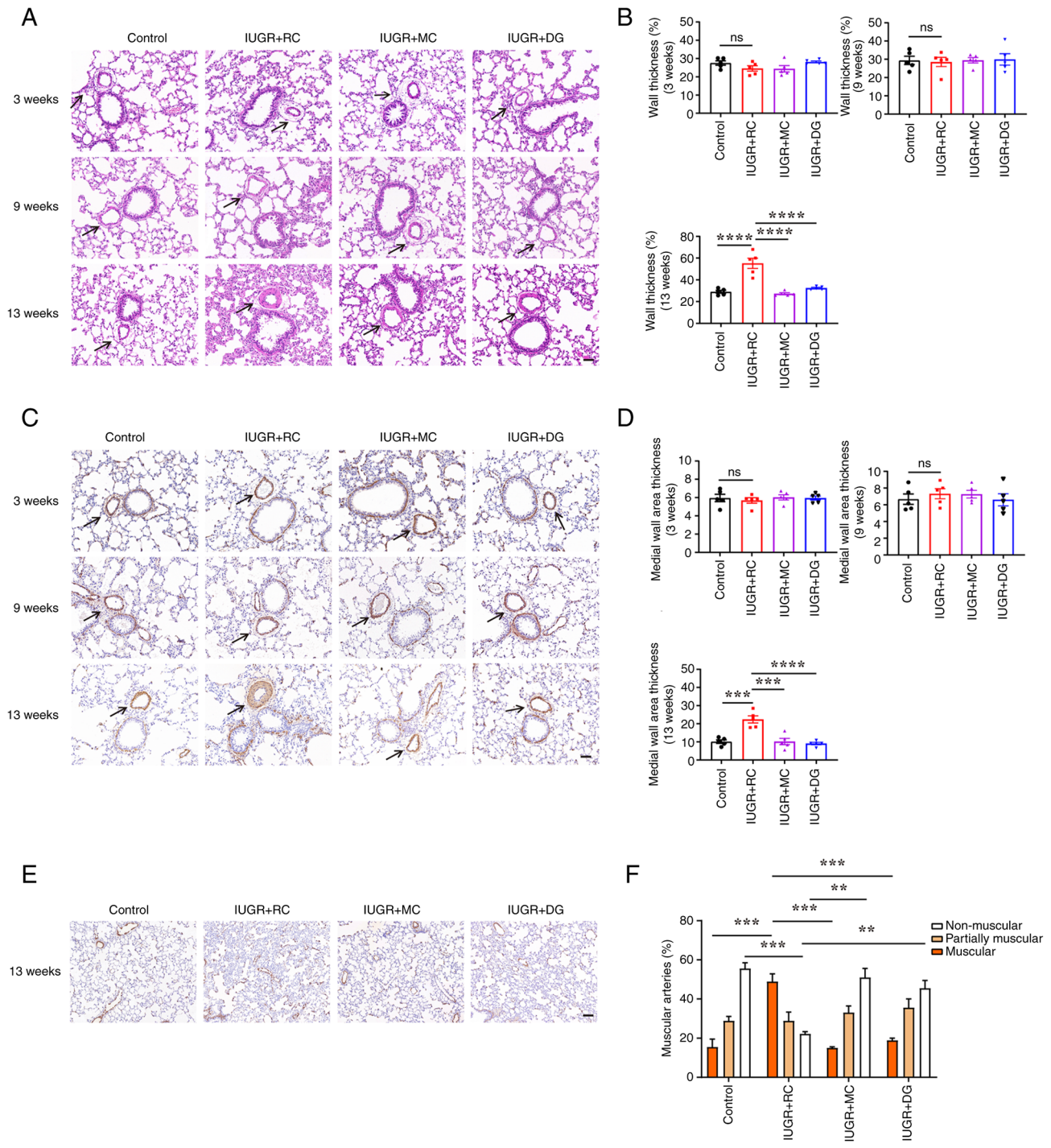

Figure 4. Continued.

were more prone to undergo apoptosis in a low-serum environment (Fig. 6B). Collectively, these data suggested that the excessive proliferation, migration and anti-apoptotic phenotype of PASMCs are among the primary contributing factors to the medial thickening and luminal narrowing observed in pulmonary arterioles during postnatal rapid catch-up growth in adult IUGR. However, these changes in PASMCs were not as pronounced in the group of rats with moderate catch-up growth.

Moderate catch-up growth prevents excessive proliferation of PVECs compared with rapid catch-up growth. Whether the remodeling of pulmonary arterioles is associated with functional changes in endothelial cells was next assessed by culturing and identifying primary PVECs. Under an optical microscope, primary rat PVECs appeared as tightly connected cobblestone-like cells. Immunofluorescence staining for CD31 showed a cell purity of ~97.6% (Fig. 6C), indicating successful isolation and cultivation of primary PVECs. The results of the EdU cell proliferation assay showed that the proliferative ability of PVECs in the IUGR + RC group was stronger than that in the control group (Fig. 6D). The proliferative ability of cells in the IUGR + MC and IUGR + DG groups showed a trend of upregulation compared with the control group,

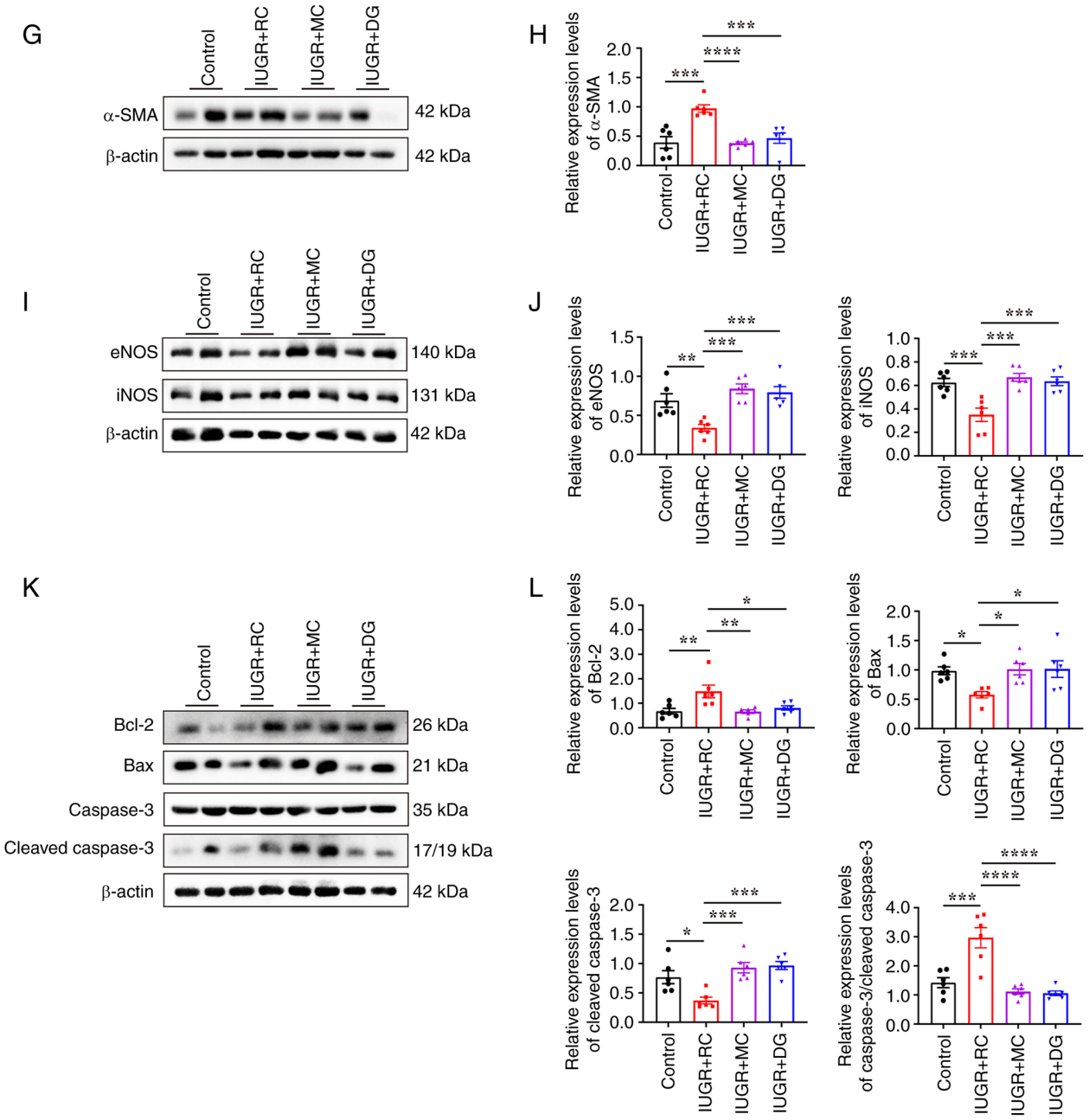

Figure 4. Rapid catch-up growth leads to pulmonary artery remodeling, and downregulation of pulmonary NOS and apoptotic proteins in adult IUGR rats. (A) Representative images of hematoxylin and eosin-stained pulmonary arterioles at three different time points. Scale bar, 50 μm. The black arrows indicate the pulmonary arterioles (diameter, 20-100 μm). (B) Quantitative analysis of medial thickness as a percentage of vessel diameter (n=5/group). (C) Representative images of α-SMA immunohistochemical staining of pulmonary arterioles at three different time points. Scale bar, 50 μm. The black arrows indicate the pulmonary arterioles (diameter range, 20-100 μm). (D) Quantitative analysis of α-SMA-positive medial thickness (n=5/group). (E) Representative images of small vessels around alveolar walls or bronchioles in 13-week-old rats. Scale bar, 100 μm. (F) Quantitative analysis of the percentage of muscularized vessels (n=3/group, with 30 vessels selected per rat). (G) Western blotting and (H) semi-quantitative analysis of α-SMA protein expression in the lung tissues of 13-week-old rats (n=6/group). (I) Western blotting and (J) semi-quantitative analysis of eNOS and iNOS protein expression in the lung tissues of 13-week-old rats (n=6/group). (K) Western blotting and (L) semi-quantitative analysis of Bcl-2, Bax, caspase-3 and cleaved caspase-3 protein expression in the lung tissues of 13-week-old rats (n=6/group). Data were analyzed using one-way ANOVA followed by Tukey's post hoc test. Data are presented as the mean ± SEM. *P<0.05, **P<0.01, ***P<0.001, ****P<0.0001. ns, not significant; IUGR, intrauterine growth restriction; RC, rapid postnatal catch-up growth; MC, moderate postnatal catch-up growth; DG, delayed growth in early postnatal life; eNOS, endothelial nitric oxide synthase; iNOS, inducible nitric oxide synthase.

although the difference was not significant. Additionally, there were no significant differences in proliferation between the IUGR + MC and IUGR + DG groups compared to the IUGR + RC group (Fig. 6D). Taken together, these results demonstrated that the excessive proliferation of PVECs served an important role in the elevation of PAP caused by rapid catch-up growth in adulthood.

Discussion

The present study demonstrated that both young and adult IUGR rats performed better in the Y-maze test than the delayed growth group, regardless of whether they experienced moderate or rapid catch-up growth. Furthermore, it was revealed that the proliferation of neural stem cells in the

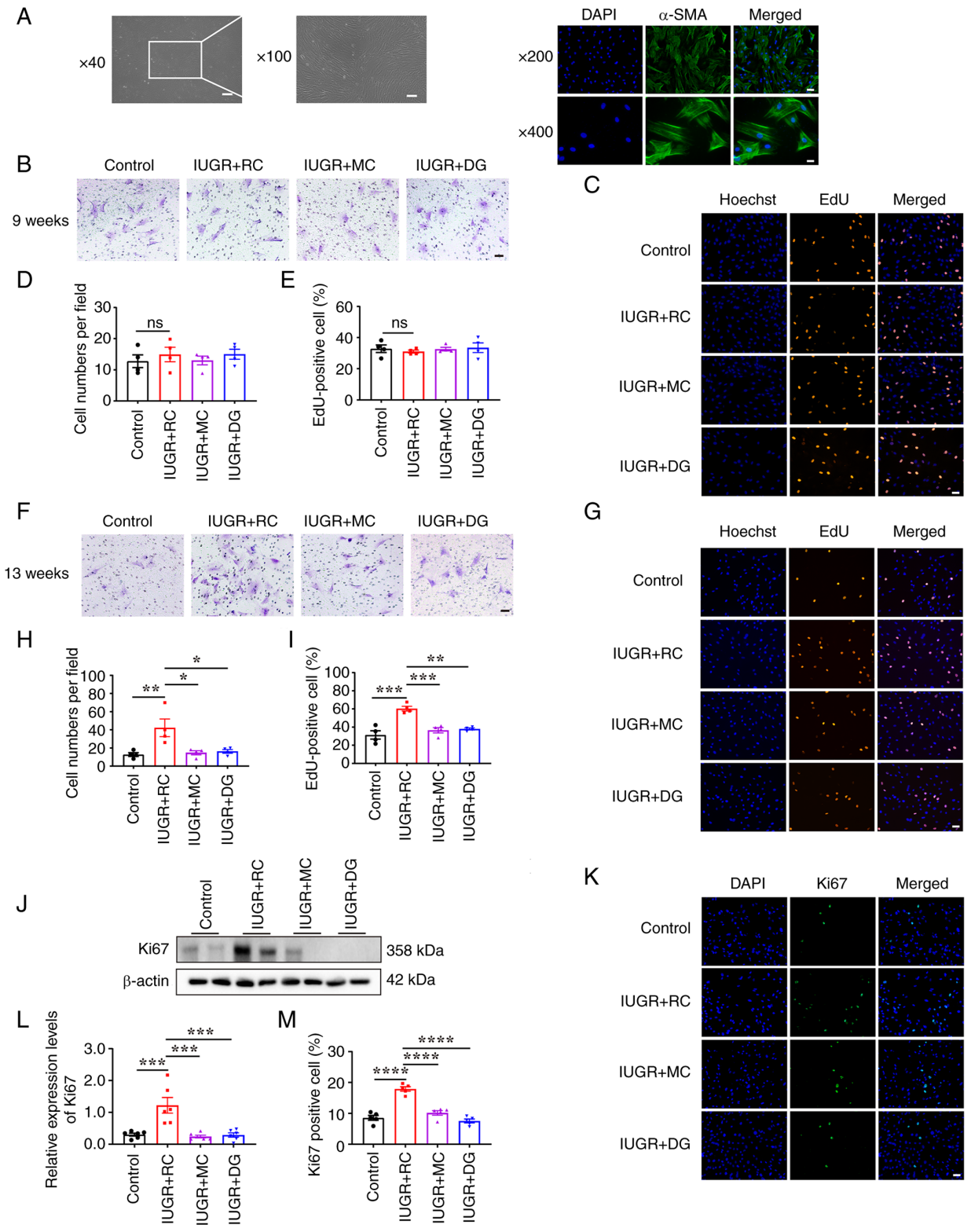

Figure 5. Rapid catch-up growth in IUGR rats leads to excessive proliferation and migration of PASMCs in adulthood. (A) Identification of primary PASMCs in rats. Light microscopy image (scale bar, 250 μm at x40 magnification; scale bar, 100 μm at x100 magnification) and α-SMA fluorescence image (scale bar, 50 μm at x200 magnification; scale bar, 25 μm at x400 magnification). (B) Transwell assay of PASMCs extracted from 9-week-old rats (scale bar, 50 μm). (C) EdU proliferation assay of PASMCs extracted from 9-week-old rats (scale bar, 50 μm). (D) Quantitative analysis of the results of the Transwell assay using the PASMCs from 9-week-old rats (n=4/group). (E) Quantitative analysis of the percentage of EdU-positive PASMCs from 9-week-old rats (n=4/group). (F) Transwell assay of PASMCs extracted from 13-week-old rats (scale bar, 50 μm). (G) EdU proliferation assay of PASMCs extracted from 13-week-old rats (scale bar, 50 μm). (H) Quantitative analysis of the Transwell assay results in 13-week-old PASMCs (n=4/group). (I) Quantitative analysis of the percentage of EdU-positive PASMCs from 13-week-old rats (n=4/group). (J) Representative western blotting images of Ki67 protein expression in primary PASMCs isolated from 13-week-old rats. (K) Representative immunofluorescence staining images for Ki67 in primary PASMCs. (L) Semi-quantitative analysis of Ki67 protein levels based on the western blotting shown in J (n=6/group). (M) Quantitative analysis of Ki67 immunofluorescence staining in primary PASMCs (n=5/group). Data were analyzed using one-way ANOVA followed by Tukey's post hoc test. Data are presented as the mean ± SEM. *P<0.05, **P<0.01, ***P<0.001, ****P<0.0001. ns, not significant; IUGR, intrauterine growth restriction; RC, rapid postnatal catch-up growth; MC, moderate postnatal catch-up growth; DG, delayed growth in early postnatal life; PASMCs, pulmonary artery smooth muscle cells.

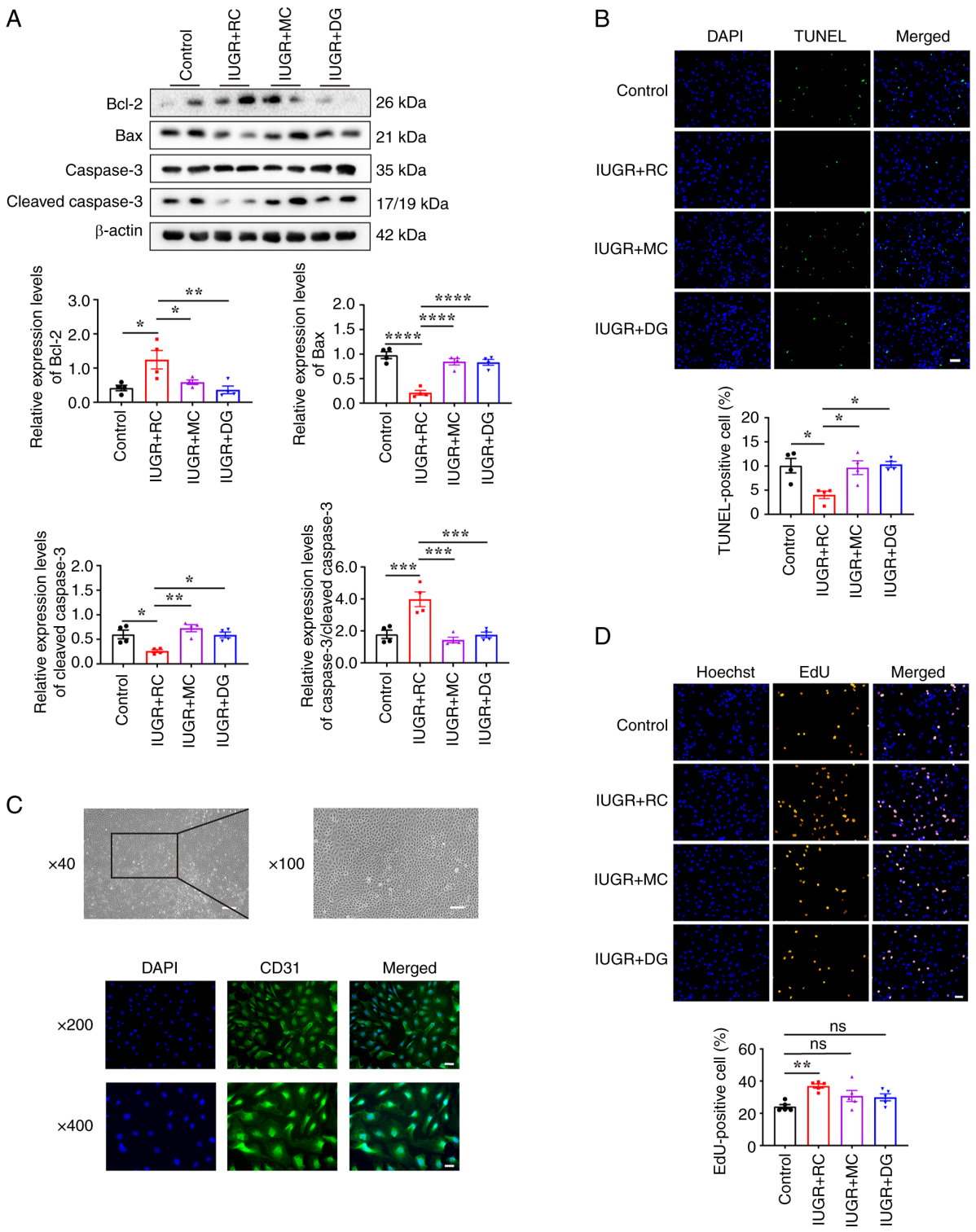

Figure 6. PASMCs from adult IUGR + RC rats exhibit an enhanced anti-apoptotic capacity and PVECs exhibit excessive proliferation. (A) Western blotting and semi-quantitative analysis of apoptosis-related proteins Bcl-2, Bax, caspase-3 and cleaved caspase-3 in PASMCs extracted from 13-week-old rats (n=4/group). (B) TUNEL staining and quantitative analysis of PASMCs treated with low serum for 48 h (n=4/group; scale bar, 50 μm). (C) Identification of primary PVECs from rats using light microscopy (scale bar, 250 μm at x40; scale bar, 100 μm at x100) and CD31 immunofluorescence staining (scale bar, 50 μm at x200; scale bar, 25 μm at x400). (D) Representative image and quantitative analysis of EdU incorporation in PVECs extracted from 13-week-old rats (n=5/group; scale bar, 50 μm). Data were analyzed using one-way ANOVA followed by Tukey's post hoc test. Data are presented as the mean ± SEM. *P<0.05, **P<0.01, ***P<0.001, ****P<0.0001. ns, not significant; IUGR, intrauterine growth restriction; RC, rapid postnatal catch-up growth; MC, moderate postnatal catch-up growth; DG, delayed growth in early postnatal life; PASMCs, pulmonary artery smooth muscle cells; PVECs, pulmonary vascular endothelial cells.

SGZ of the hippocampus was reduced in the delayed growth group. Conversely, experiencing rapid catch-up growth during lactation increased susceptibility to cardiovascular disease in adulthood; this included increased mPAP, medial thickening of pulmonary arterioles, luminal narrowing and increased muscularization of pulmonary small vessels. Furthermore, PASMCs

exhibited excessive proliferation, enhanced migratory ability and anti-apoptotic activity. Similarly, PVECs exhibited excessive proliferation. By contrast, moderate catch-up growth and delayed growth in IUGR rats did not result in negative effects on cardiovascular function. It was also observed that these adverse cardiovascular outcomes caused by rapid catch-up growth only occurred during adulthood. Thus, the present study provides experimental evidence that moderate catch-up growth following IUGR is superior to rapid catch-up growth or delayed growth, particularly in promoting optimal pulmonary vascular function and memory function in adulthood. These findings provide a research foundation for developing appropriate feeding patterns for infants with IUGR.

Research has shown that providing sufficient nutrition during the perinatal period is crucial for neurodevelopment, which is necessary to support the growth and development of nerve cells (39). Throughout the life of adult mammals, neurogenesis occurs in the brain, and neural stem cells are present in the subventricular zone of the lateral ventricles and the SGZ of the dentate gyrus in the hippocampus. These neural stem cells can continuously generate new neurons and integrate them into local neural circuits (40,41). Ki67 is a nuclear protein that can be used as a marker to determine the state of a cell in the cell cycle, with its expression varying in the different stages of the cell cycle. It also serves as an indicator of neural stem cell proliferation status (42). In the development and repair of the nervous system, Ki67 is widely used for the identification and analysis of neural stem cells and neural progenitor cells (43). In our previous study, it was demonstrated that IUGR accompanied by delayed postnatal growth affects the expression of memory-related gene zif268 and transcription factor recruitment factor p300 in the hippocampus and leads to a decrease in synaptic plasticity in the CA1 region. This, in turn, causes irreversible damage to the cognitive function of adult rats (14). In the present study, it was further revealed that delayed growth affected the number of Ki67-positive neural stem cells in the SGZ region of IUGR rats. Therefore, catch-up growth is beneficial for brain development. This process can increase the proliferation of neural stem cells in the hippocampus and improve memory deficits caused by IUGR.

The 'Developmental Origins of Health and Disease' theory states that the degree of growth in the early stages of life and nutritional exposure have an impact on chronic diseases in adulthood (44). When it comes to cardiovascular function, the results of the present study showed that only the IUGR + RC group exhibited an increase in mPAP in adulthood, whereas mRVP and RVHI did not change. These results suggested that the increase in mPAP in the IUGR + RC group was temporary and had not yet affected right ventricular function. Therefore, there was no evidence of right ventricular hypertrophy. However, this does not mean that catch-up growth does not lead to right ventricular dysfunction, and longer-term experiments are required to verify this. Research has shown that IUGR increases the risk of hypertension in adults (45,46). A clinical study by Leunissen *et al* (47) reported that childhood weight gain, especially fat mass, not birth weight, determines blood pressure in young adults. However, in the present study, neither catch-up growth nor postnatal nutritional restriction led to an increase in mAAP at all time points, which represents systemic circulation pressure. A possible reason is that the subjects were still too young to exhibit changes in systemic circulation pressure.

Endothelial cell dysfunction, characterized by an imbalanced production of vasoconstrictors and vasodilators, and a reduced availability of bioactive NO, is considered a crucial underlying factor in various clinical and experimental forms of pulmonary hypertension (48). In the present study of the mechanism underlying adult PAH caused by rapid catch-up growth, it was observed that the IUGR + RC group exhibited an increase in smooth muscle layer thickness in the pulmonary arteries, narrowed vascular lumens and a higher proportion of muscularization in pulmonary small vessels. Notably, these histopathological changes did not occur in the IUGR + MC group during adulthood. In addition, the protein expression levels of eNOS and iNOS in the lungs of the IUGR + RC group were decreased during adulthood, potentially resulting in a decrease in NO production in the lungs. NO is not only an effective pulmonary vasodilator, but it also prevents hypoxia-induced pulmonary vasoconstriction (49), inhibits smooth muscle proliferation and platelet aggregation (50), and downregulates ET-1 production (51). The decrease in the expression of these NOSs may have an important role in the elevated PAP.

Previous studies have shed light on the underlying mechanism of PAH, revealing that the primary cause of its persistent progression and resistance to treatment lies in pulmonary vascular remodeling (52,53), which is primarily caused by medial hypertrophy and the formation of neointimal lesions. Apoptosis resistance, proliferation and migration of PASMCs also serve a vital role in this process (36). In the present study, PASMCs extracted from the lungs of 13-week-old rats exhibited enhanced proliferative and migratory abilities under normal oxygen conditions. TUNEL results also revealed that PASMCs in the IUGR + RC group exhibited anti-apoptotic properties in a low serum, pro-apoptotic 'starvation' environment. In addition, disordered proliferation of endothelial cells accompanied by neovascularization is a common pathological feature of pulmonary vessels in patients with PAH (54). In the present study, it was found that PVECs extracted from the lungs of IUGR + RC adult rats exhibited increased proliferation. Dysfunction of these PASMCs and PVECs resulted in remodeling of the pulmonary arterioles, ultimately leading to elevated mPAP in adult IUGR rats after rapid catch-up growth. By contrast, the rats in the IUGR + MC and IUGR + DG groups did not exhibit dysfunction in these cells. These findings support the notion that a discrepancy between early life experiences and the intrauterine environment can result in cardiovascular dysfunction (44). All of these results demonstrated that moderate catch-up growth after birth is more beneficial for children with IUGR to achieve appropriate cardiovascular and cognitive function in adulthood.

Based on our previous findings that delayed postnatal growth leads to cognitive impairment but reverses the elevations in mPAP induced by postnatal catch-up growth (14). Since no distinction was made regarding the rate of catch-up growth, it is evident that this result has limitations. Therefore, we aimed to assess new postnatal nutritional strategies to maintain optimal pulmonary vascular function in adult individuals with a history of IUGR without compromising

essential brain functions. Building upon this preliminary research, an animal model of moderate catch-up growth was established. The innovative aspect of the present study was the investigation of the effects of various early-life nutritional interventions on the short-term and long-term health outcomes of IUGR rats, without being restricted to a single time period. To the best of our knowledge, the present study is the first to demonstrate the superiority of moderate catch-up growth as a postnatal nutritional pattern in terms of both cognitive function and pulmonary vascular function. The findings suggested that adopting a strategy of moderate catch-up growth in nutritional interventions for children with IUGR may result in improved health outcomes. This discovery provides guidance for clinical practice and postnatal intervention measures in managing IUGR. However, the present study has certain limitations. There was a focus on the effects of moderate catch-up growth on the pulmonary vascular and memory functions of rats. However, the issues of glucose and lipid metabolism caused by rapid catch-up growth cannot be ignored. Further research is required to determine whether postnatal moderate catch-up growth also leads to insulin resistance and obesity. The mechanisms underlying the impact of IUGR on memory function also require further investigation. Additionally, it is crucial to investigate the mechanisms that contribute to the dysfunction of rat PASMCs and PVECs in response to rapid catch-up growth. Notably, the offspring of IUGR rats in the present study were generated from dams that experienced prenatal nutritional restriction. As aforementioned, the causes of IUGR include genetic factors, fetal factors, placental factors and maternal health factors (2,3). The conclusions in the present study only apply to IUGR caused by maternal health issues, rather than all types of IUGR.

Taken together, the present findings suggested that different catch-up growth patterns after IUGR have significant long-term health effects. Notably, moderate catch-up growth may be a more favorable option. Moderate catch-up growth appears to be a healthier approach to catch-up growth, which may enable children with IUGR to achieve improved cognitive function and pulmonary vascular function in adulthood. These results highlight the importance of considering healthier catch-up growth patterns in the postnatal management of IUGR and provide insights into potential strategies to improve long-term outcomes in these individuals.

Acknowledgements

The authors would like to thank Dr Chao Chen (Zhejiang University) for their assistance with measuring pulmonary artery pressure.

Funding

The present study was funded by the National Natural Science Foundation of China (grant nos. 81630037 and 82241017).

Availability of data and materials

The data generated in the present study may be requested from the corresponding author.

Authors' contributions

LY and LD conceived the present study. LY performed data curation. Conception and design were the responsibility of LY and YH. CH, KC, YY and LZ were responsible for the analysis and interpretation of data. LY and LD were responsible for supervision and project administration, and writing, reviewing and editing the manuscript. Data visualization was the responsibility of XL. LY wrote the original draft of the manuscript. LD was responsible for funding acquisition. LY and YH confirm the authenticity of all the raw data. All authors read and approved the final manuscript.

Ethics approval and consent to participate

The animal study protocol was approved by the Animal Care and Use Committee of Zhejiang University (approval no. ZJU20160215; Hangzhou, China).

Patient consent for publication

Not applicable.

Competing interests

The authors declare that they have no competing interests.

References

1. Kesavan K and Devaskar SU: Intrauterine growth restriction: Postnatal monitoring and outcomes. Pediatr Clin North Am 66: 403-423, 2019.
2. Sharma D, Shastri S, Farahbakhsh N and Sharma P: Intrauterine growth restriction-part 1. J Matern Fetal Neonatal Med 29: 3977-3987, 2016.
3. Bernstein PS and Divon MY: Etiologies of fetal growth restriction. Clin Obstet Gynecol 40: 723-729, 1997.
4. Rosenberg A: The IUGR newborn. Semin Perinatol 32: 219-224, 2008.
5. Chernausek SD: Update: Consequences of abnormal fetal growth. J Clin Endocrinol Metab 97: 689-695, 2012.
6. Longo S, Bollani L, Decembrino L, Di Comite A, Angelini M and Stronati M: Short-term and long-term sequelae in intrauterine growth retardation (IUGR). J Matern Fetal Neonatal Med 26: 222-225, 2013.
7. Tomi M, Zhao Y, Thamotharan S, Shin BC and Devaskar SU: Early life nutrient restriction impairs blood-brain metabolic profile and neurobehavior predisposing to Alzheimer's disease with aging. Brain Res 1495: 61-75, 2013.
8. An J, Wang J, Guo L, Xiao Y, Lu W, Li L, Chen L, Wang X and Dong Z: The impact of gut microbiome on metabolic disorders during catch-up growth in small-for-gestational-age. Front Endocrinol (Lausanne) 12: 630526, 2021.
9. Lee PA, Chernausek SD, Hokken-Koelega AC and Czernichow P; International Small for Gestational Age Advisory Board: International small for gestational age advisory board consensus development conference statement: Management of short children born small for gestational age, April 24-October 1, 2001. Pediatrics 111: 1253-1261, 2003.
10. Ong KK: Catch-up growth in small for gestational age babies: Good or bad? Curr Opin Endocrinol Diabetes Obes 14: 30-34, 2007.
11. Eriksson JG, Forsén T, Tuomilehto J, Winter PD, Osmond C and Barker DJ: Catch-up growth in childhood and death from coronary heart disease: Longitudinal study. BMJ 318: 427-431, 1999.
12. Berends LM, Fernandez-Twinn DS, Martin-Gronert MS, Cripps RL and Ozanne SE: Catch-up growth following intra-uterine growth-restriction programmes an insulin-resistant phenotype in adipose tissue. Int J Obes (Lond) 37: 1051-1057, 2013.

13. Ong KK, Ahmed ML, Emmett PM, Preece MA and Dunger DB: Association between postnatal catch-up growth and obesity in childhood: Prospective cohort study. BMJ 320: 967-971, 2000.
14. Yan L, Wang Y, Zhang Z, Xu S, Ullah R, Luo X, Xu X, Ma X, Chen Z, Zhang L, *et al*: Postnatal delayed growth impacts cognition but rescues programmed impaired pulmonary vascular development in an IUGR rat model. Nutr Metab Cardiovasc Dis 29: 1418-1428, 2019.
15. Rueda-Clausen CF, Morton JS and Davidge ST: Effects of hypoxia-induced intrauterine growth restriction on cardiopulmonary structure and function during adulthood. Cardiovasc Res 81: 713-722, 2009.
16. Kuo AH, Li C, Huber HF, Schwab M, Nathanielsz PW and Clarke GD: Maternal nutrient restriction during pregnancy and lactation leads to impaired right ventricular function in young adult baboons. J Physiol 595: 4245-4260, 2017.
17. Mericq V, Martinez-Aguayo A, Uauy R, Iñiguez G, Van der Steen M and Hokken-Koelega A: Long-term metabolic risk among children born premature or small for gestational age. Nat Rev Endocrinol 13: 50-62, 2017.
18. Kelishadi R, Haghdoost AA, Jamshidi F, Aliramezany M and Moosazadeh M: Low birthweight or rapid catch-up growth: Which is more associated with cardiovascular disease and its risk factors in later life? A systematic review and cryptanalysis. Paediatr Int Child Health 35: 110-123, 2015.
19. Zhang Z, Luo X, Lv Y, Yan L, Xu S, Wang Y, Zhong Y, Hang C, Jyotsnav J, Lai D, *et al*: Intrauterine growth restriction programs intergenerational transmission of pulmonary arterial hypertension and endothelial dysfunction via sperm epigenetic modifications. Hypertension 74: 1160-1171, 2019.
20. Luo X, Hang C, Zhang Z, Le K, Ying Y, Lv Y, Yan L, Huang Y, Ye L, Xu X, *et al*: PVECs-derived exosomal microRNAs regulate PASMCs via FoxM1 signaling in IUGR-induced pulmonary hypertension. J Am Heart Assoc 11: e027177, 2022.
21. Lv Y, Tang LL, Wei JK, Xu XF, Gu W, Fu LC, Zhang LY and Du LZ: Decreased Kv1.5 expression in intrauterine growth retardation rats with exaggerated pulmonary hypertension. Am J Physiol Lung Cell Mol Physiol 305: L856-L865, 2013.
22. Dabral S, Tian X, Kojonazarov B, Savai R, Ghofrani HA, Weissmann N, Florio M, Sun J, Jonigk D, Maegel L, *et al*: Notch1 signalling regulates endothelial proliferation and apoptosis in pulmonary arterial hypertension. Eur Respir J 48: 1137-1149, 2016.
23. Courboulin A, Barrier M, Perreault T, Bonnet P, Tremblay VL, Paulin R, Tremblay E, Lambert C, Jacob MH, Bonnet SN, *et al*: Plumbagin reverses proliferation and resistance to apoptosis in experimental PAH. Eur Respir J 40: 618-629, 2012.
24. Jimenez-Chillaron JC and Patti ME: To catch up or not to catch up: Is this the question? Lessons from animal models. Curr Opin Endocrinol Diabetes Obes 14: 23-29, 2007.
25. National Research Council: Committee for the Update of the Guide for the Care and Use of Laboratory Animals: Guide for the Care and Use of Laboratory Animals. 8th edition. National Academies Press, Washington, DC, 2011.
26. Xu XF, Lv Y, Gu WZ, Tang LL, Wei JK, Zhang LY and Du LZ: Epigenetics of hypoxic pulmonary arterial hypertension following intrauterine growth retardation rat: Epigenetics in PAH following IUGR. Respir Res 14: 20, 2013.
27. Barrow PC, Barbellion S and Stadler J: Preclinical evaluation of juvenile toxicity. Methods Mol Biol 691: 17-35, 2011.
28. Shokouhi G, Kosari-Nasab M and Salari AA: Silymarin sex-dependently improves cognitive functions and alters TNF-α, BDNF, and glutamate in the hippocampus of mice with mild traumatic brain injury. Life Sci 257: 118049, 2020.
29. Olofinnade AT, Adeyeba A, Onaolapo AY and Onaolapo OJ: An assessment of the effects of azodicarbonamide-containing diet on neurobehaviour, brain antioxidant status and membrane lipid peroxidation status in rats. Cent Nerv Syst Agents Med Chem 20: 49-57, 2020.
30. Sadiki FZ, Idrissi ME, Cioanca O, Trifan A, Hancianu M, Hritcu L and Postu PA: Tetraclinis articulata essential oil mitigates cognitive deficits and brain oxidative stress in an Alzheimer's disease amyloidosis model. Phytomedicine 56: 57-63, 2019.
31. Abdulbasit A, Stephen Michael F, Shukurat Onaopemipo A, Abdulmusawwir AO, Aminu I, Nnaemeka Tobechukwu A, Wahab Imam A, Oluwaseun Aremu A, Folajimi O, Bilikis Aderonke A, *et al*: Glucocorticoid receptor activation selectively influence performance of Wistar rats in Y-maze. Pathophysiology 25: 41-50, 2018.
32. Xu YP, Zhu JJ, Cheng F, Jiang KW, Gu WZ, Shen Z, Wu YD, Liang L and Du LZ: Ghrelin ameliorates hypoxia-induced pulmonary hypertension via phospho-GSK3 β/β-catenin signaling in neonatal rats. J Mol Endocrinol 47: 33-43, 2011.
33. Luo F, Wang X, Luo X, Li B, Zhu D, Sun H and Tang Y: Invasive hemodynamic assessment for the right ventricular system and hypoxia-induced pulmonary arterial hypertension in mice. J Vis Exp 24, 2019.
34. Wang Q, Shi W, Zhang Q, Feng W, Wang J, Zhai C, Yan X and Li M: Inhibition of Siah2 ubiquitin ligase ameliorates monocrotaline-induced pulmonary arterial remodeling through inactivation of YAP. Life Sci 242: 117159, 2020.
35. Jones R, Jacobson M and Steudel W: alpha-smooth-muscle actin and microvascular precursor smooth-muscle cells in pulmonary hypertension. Am J Respir Cell Mol Biol 20: 582-594, 1999.
36. Huang S, Yue Y, Feng K, Huang X, Li H, Hou J, Yang S, Huang S, Liang M, Chen G and Wu Z: Conditioned medium from M2b macrophages modulates the proliferation, migration, and apoptosis of pulmonary artery smooth muscle cells by deregulating the PI3K/Akt/FoxO3a pathway. PeerJ 8: e9110, 2020.
37. Nie X, Dai Y, Tan J, Chen Y, Qin G, Mao W, Zou J, Chang Y, Wang Q and Chen J: α-Solanine reverses pulmonary vascular remodeling and vascular angiogenesis in experimental pulmonary artery hypertension. J Hypertens 35: 2419-2435, 2017.
38. Ye L, Wang X, Cai C, Zeng S, Bai J, Guo K, Fang M, Hu J, Liu H, Zhu L, *et al*: FGF21 promotes functional recovery after hypoxic-ischemic brain injury in neonatal rats by activating the PI3K/Akt signaling pathway via FGFR1/β-kloth. Exp Neurol 317: 34-50, 2019.
39. Prado EL and Dewey KG: Nutrition and brain development in early life. Nutr Rev 72: 267-284, 2014.
40. Bond Allison M, Ming G-l and Song H: Adult mammalian neural stem cells and neurogenesis: Five decades later. Cell Stem Cell 17: 385-395, 2015.
41. Zhao C, Deng W and Gage FH: Mechanisms and functional implications of adult neurogenesis. Cell 132: 645-660, 2008.
42. Scholzen T and Gerdes J: The Ki-67 protein: From the known and the unknown. J Cell Physiol 182: 311-322, 2000.
43. Wojtowicz JM and Kee N: BrdU assay for neurogenesis in rodents. Nat Protoc 1: 1399-1405, 2006.
44. Bateson P, Gluckman P and Hanson M: The biology of developmental plasticity and the predictive adaptive response hypothesis. J Physiol 592: 2357-2368, 2014.
45. Amruta N, Kandikattu HK and Intapad S: Cardiovascular dysfunction in intrauterine growth restriction. Curr Hypertens Rep 24: 693-708, 2022.
46. Gortner L: Intrauterine growth restriction and risk for arterial hypertension: A causal relationship? J Perinat Med 35: 361-365, 2007.
47. Leunissen RWJ, Kerkhof GF, Stijnen T and Hokken-Koelega ACS: Effect of birth size and catch-up growth on adult blood pressure and carotid intima-media thickness. Horm Res Paediatr 77: 394-401, 2012.
48. Teichert-Kuliszewska K, Tsoporis JN, Desjardins JF, Yin J, Wang L, Kuebler WM and Parker TG: Absence of the calcium-binding protein, S100A1, confers pulmonary hypertension in mice associated with endothelial dysfunction and apoptosis. Cardiovasc Res 105: 8-19, 2015.
49. Perrella MA, Edell ES, Krowka MJ, Cortese DA and Burnett JC Jr: Endothelium-derived relaxing factor in pulmonary and renal circulations during hypoxia. Am J Physiol 263: R45-R50, 1992.
50. Dinh-Xuan AT: Endothelial modulation of pulmonary vascular tone. Eur Respir J 5: 757-762, 1992.
51. Smith AP, Demoncheaux EA and Higenbottam TW: Nitric oxide gas decreases endothelin-1 mRNA in cultured pulmonary artery endothelial cells. Nitric Oxide 6: 153-159, 2002.
52. Thompson AAR and Lawrie A: Targeting vascular remodeling to treat pulmonary arterial hypertension. Trends Mol Med 23: 31-45, 2017.
53. Ruopp NF and Cockrill BA: Diagnosis and treatment of pulmonary arterial hypertension: A review. JAMA 327: 1379-1391, 2022.
54. Budhiraja R, Tuder RM and Hassoun PM: Endothelial dysfunction in pulmonary hypertension. Circulation 109: 159-165, 2004.